



INSTITUT DE FRANCE
Académie des sciences

Comptes Rendus

Chimie

Carmen Ciotonea, Alexandru Chirieac, Brindusa Dragoi, Cezar Catrinescu, Sébastien Royer and Adrian Ungureanu

Cu–Ga₂O₃ nanoparticles supported on ordered mesoporous silica for the catalytic hydrogenation of cinnamaldehyde


Volume 25, Special Issue S3 (2022), p. 81-94

Published online: 22 February 2022

<https://doi.org/10.5802/crchim.141>

Part of Special Issue: Active site engineering in nanostructured materials for energy, health and environment

Guest editors: Ioana Fechete (Université de Troyes, France) and Doina Lutic (Al. I. Cuza University of Iasi, Romania)

 This article is licensed under the
CREATIVE COMMONS ATTRIBUTION 4.0 INTERNATIONAL LICENSE.
<http://creativecommons.org/licenses/by/4.0/>



*Les Comptes Rendus. Chimie sont membres du
Centre Mersenne pour l'édition scientifique ouverte*
www.centre-mersenne.org
e-ISSN : 1878-1543



Active site engineering in nanostructured materials for energy, health and environment /
*Ingénierie de sites actifs dans les matériaux nanostructurés pour l'énergie, la santé et
l'environnement*

Cu–Ga₂O₃ nanoparticles supported on ordered mesoporous silica for the catalytic hydrogenation of cinnamaldehyde

Nanoparticules Cu-Ga₂O₃ supportées sur de la silice mésoporeuse ordonnée pour l'hydrogénation catalytique du cinnamaldéhyde

Carmen Ciotonea^{ⓧ a, b, c}, Alexandru Chiriac^a, Brindusa Dragoi^a, Cezar Catrinescu^{ⓧ a}, Sébastien Royer^{ⓧ *, b} and Adrian Ungureanu^{ⓧ *, a}

^a “Gheorghe Asachi” Technical University of Iasi, Faculty of Chemical Engineering and Environmental Protection “Cristofor Simionescu”, 73, Prof. D. Mangeron Blvd., 700050 Iasi, Romania

^b Univ. Lille, CNRS, Centrale Lille, Univ. Artois, UMR 8181 – UCCS – Unité de Catalyse et Chimie du Solide, F-59000 Lille, France

^c Université du Littoral Côte d'Opale, Unité de Chimie Environnementale et Interactions sur le Vivant (UCEIV), UR4492, SFR Condorcet FR CNRS 3417, 145, Avenue Maurice Schumann, 59140 Dunkerque, France

E-mails: carmen.ciotonea@univ-lille.fr (C. Ciotonea), alexandruchiriac_is@yahoo.com (A. Chiriac), brindusa.dragoi@yahoo.com (B. Dragoi), ccatrine@tuiasi.ro (C. Catrinescu), sebastien.royer@univ-lille.fr (S. Royer), aungureanu@tuiasi.ro (A. Ungureanu)

Dedicated to render homage to the scientific work of Professor Emil Dumitriu

Abstract. Herein, we show that gallium oxide can function as an efficient promoter for the Cu-catalysed hydrogenation of cinnamaldehyde. SBA-15-supported Cu–Ga₂O₃ nanoparticles with a constant Cu loading of 5 wt% and two Cu/Ga weight ratios of 5 and 2, respectively, were synthesised by incipient wetness impregnation followed by mild drying. Physico-chemical characterisation revealed that the metal dispersion, and thus the active surface area of copper, can be enhanced nine-fold upon the addition of gallium promoter, boosting the catalytic activity as compared with the unpromoted Cu/SBA-15 catalyst. Likewise, the presence of Ga₂O₃ improved the selectivity to cinnamyl alcohol.

* Corresponding authors.

Résumé. Ce travail montre que l'oxyde de gallium est un promoteur efficace pour l'hydrogénation du cinnamaldéhyde catalysée par le cuivre. Des nanocatalyseurs Cu-Ga₂O₃ supportés sur SBA-15, avec une teneur en Cu constante (5% pds) et deux rapports massiques Cu/Ga (5 et 2), ont été préparés par imprégnation à humidité naissante — séchage en conditions douces. Les caractérisations physico-chimiques réalisées montrent que la dispersion de la phase métallique et donc la surface active du Cu, peut être augmentée d'un facteur 9 par l'addition du promoteur. Cela permet d'atteindre des activités catalytiques améliorées par rapport au catalyseur Cu/SBA-15. La présence de Ga₂O₃ permet également d'augmenter la sélectivité en alcool cinnamique.

Keywords. Copper, Gallium, Nanoparticles, SBA-15, Hydrogenation, Cinnamaldehyde.

Mots-clés. Cuivre, Gallium, Nanoparticules, SBA-15, Hydrogénation, Cinnamaldéhyde.

Published online: 22 February 2022

1. Introduction

Supported metal nanoparticles (MNPs), both noble (e.g., Pt, Pd, Au) and non-noble (e.g., Co, Ni, Cu), are widely used as hydrogenation catalysts for the production of bulk chemicals, fine chemicals, clean fuels and removal of pollutants [1,2]. For such applications, the catalysts are usually tailored under the form of nanosized metal particles carried by porous oxide supports [3]. It has been reviewed that many factors, including the particle size, shape, chemical composition and oxidation state, metal-support interaction, and metal-reactant/solvent interaction can influence the catalytic performances of supported MNPs [4,5]. For instance, decreasing the particle size of MNPs in the small range (<5 nm) can greatly enhance the metal dispersion, and thus the active surface area exposed to reactants, which boost the catalytic performance [6,7].

Among various supported MNPs, the Cu NPs have generated a rapid growth of interest in catalysis because copper is relatively inexpensive and abundant in nature [8]. In this regard, supported Cu NPs show promising catalytic activity and selectivity for many important hydrogenation reactions, such as the hydrogenation of esters, carboxylic acids, ethers, furanic compounds, CO₂, and, in particular, the hydrogenation of α , β -unsaturated aldehydes, like cinnamaldehyde [8–10]. The last catalytic reaction is very interesting from a fundamental point of view (i.e., the control of chemoselectivity: C=O vs C=C bond hydrogenation) and for the fine chemicals industry, as well (i.e., the hydrogenation products: cinnamyl alcohol, hydrocinnamaldehyde, and hydrocinnamyl alcohol are used for the production of flavours and perfumes, pharmaceuticals, agrochemicals etc.) [11–14]. The control over the size and stability of the supported Cu NPs to maximize catalytic

activity is however difficult, especially at a high loading of copper on silica (≥ 5 wt%), due to the particles growth by migration and coalescence of the very mobile copper species, and Ostwald ripening upon the high-temperature catalyst calcination and reduction steps and/or operation, causing a partial or even a total loss of the active surface [15,16]. As a result, albeit copper has been introduced onto high-surface area mesoporous silica supports by incipient wetness impregnation (IWI), large Cu particles have been obtained upon calcination and reduction, with a poor dispersion of copper, a low capacity to activate H₂, and, consequently, with an insignificant catalytic performance in the hydrogenation of cinnamaldehyde [17–20].

Several strategies have been tested to mitigate the poor dispersion of Cu NPs obtained by IWI, namely controlled calcination conditions [15], drying at ambient temperature [21], IWI followed by mild drying (IWI-MD) [17,22] or vacuum-thermal treatment [23]. It is worthy of mention that IWI is still the synthesis method of choice for both academia and industry due to some sustainability-related features, including versatility, convenience, small amount of solvent (typically water), availability and low cost of metal sources (typically hydrated metal nitrates), high purity of metal precursor phases (typically metal oxides), and limited production of waste [3]. Nonetheless, the experimental results indicated that the stability of Cu NPs obtained by IWI over mesoporous silica is far from being solved. Therefore, other strategies have been proposed, such as the addition of a second metal to Cu (e.g., Ni, Cr, Co) [17,18,20,22, 24], the incorporation of Al heteroatoms into the mesoporous silica support [19], and the functionalization or pore occlusion of mesoporous silica supports by non-ionic surfactants [24–27]. This way,

a significant improvement of dispersion and catalytic performance of copper in the hydrogenation of cinnamaldehyde has been obtained. As an example, we recently reported that the incorporation of 20 wt% Al₂O₃ in the SBA-15 support structure leads to an increase of copper dispersion by a factor of 6 compared with the pure siliceous SBA-15-supported catalyst (25.6 vs 4.6%), when Cu has been introduced by IWI-MD. It means a decrease of the particle size of Cu NPs to the small-size range (from 21.6 to 3.9 nm) [19]. As consequence, a high catalytic activity was demonstrated for the cinnamaldehyde hydrogenation (TOF of $6 \times 10^{-3} \text{ s}^{-1}$ at 110 °C). Noteworthy, the incorporation of Al provided surface Lewis acidic sites that favoured the transformation of cinnamaldehyde into cinnamyl alcohol by C=O bond hydrogenation on dual metal-electron deficient Cu⁰-Al^{δ+} sites, demonstrating hence a high chemoselectivity towards the unsaturated alcohol (~50% at ~40% conversion of cinnamaldehyde), close to that of a mesoporous alumina-supported system. In another example, it has been reported that by comparison with the monometallic Cu/SBA-15, the bimetallic Cu-Cr/SBA-15 catalysts obtained by IWI-MD show improved chemoselectivity towards cinnamyl alcohol (~50%), yet at a low reaction rate (~10% conversion of cinnamaldehyde) [18]. The authors correlated the catalytic activity with the particle size of copper, whereas the high selectivity to the unsaturated alcohol has been explained by the presence of dual Cu⁰-Cr^{δ+} sites. Therefore, to design performance copper catalysts for the hydrogenation of α , β -unsaturated aldehydes, like cinnamaldehyde, it is compulsory to synthesize highly dispersed Cu⁰ sites capable to activate H₂, promoting the catalytic activity in hydrogenation, in junction with positively charged M^{δ+} metal sites, to preferentially interact, and then, activate the C=O groups of cinnamaldehyde molecule, promoting the catalytic selectivity to the unsaturated alcohol. Examples from literature validate this hypothesis (e.g., Cu-Zn-Al, Pt-Sn, Pt-Fe, Pt-Ga metal-metal oxide catalysts) [28–31].

Considering all of the above aspects, in this study we applied the IWI-MD synthesis method and we used a high-surface area ordered mesoporous SBA-15 silica support to investigate the gallium oxide promoter effect for the Cu NPs-catalysed hydrogenation of cinnamaldehyde. Emphasis was put on the effect of the Cu/Ga weight ratio on the dispersion

of copper. Ga is a *p*-block metal that has an oxidation state of +3 in most of its compounds. Previous studies revealed that Ga₂O₃ exposing Lewis acidic sites was the major phase presented on the SBA-15 silica surface after calcination, when Ga was introduced by IWI [32]. Hence, it can be possible to generate electron deficient Ga^{δ+} sites with affinity to the C=O groups, near the metallic Cu⁰ sites. There are few encouraging reports on the efficient Ga₂O₃ promotion for other Cu NPs-catalysed selective hydrogenation reactions, such as the hydrogenation of CO₂ to methanol over CuZnGaO_x [33], Cu-Ga₂O₃/ZrO₂ [34], Cu-Ga₂O₃-ZnO/ZrO₂ [35,36], Cu-Ga₂O₃/SiO₂ [37–39], Cu-Ga₂O₃-ZnO/SiO₂ [40], and Cu-Ga₂O₃-ZnO/HZSM-5 [41]. Nevertheless, the Ga₂O₃ promoter effects are little studied for the hydrogenation of α , β -unsaturated aldehydes (i.e., the hydrogenation of citral over Pt-Ga₂O₃/C, and the hydrogenation of cinnamaldehyde over Cu-Ga₂O₃/HNZY) [30,42]. A combination of XRD, TEM/EDXS, N₂ physisorption, H₂-TPR, and N₂O chemisorption analyses allowed us to correlate the structural, textural and reducible properties of the Cu-Ga₂O₃/SBA-15 nanomaterials with their catalytic performances in terms of activity and selectivity.

2. Experimental

2.1. Chemicals

All chemicals required to prepare the support and the catalysts were used as purchased: tetraethylorthosilicate (Si(OC₂H₅)₄, TEOS, 98%, Sigma-Aldrich), non-ionic triblock copolymer Pluronic P123 (poly(ethyleneoxide)-block-poly-(propyleneoxide)-block-poly(ethyleneoxide)-block, EO₂₀PO₇₀EO₂₀, molecular weight = 5800, BASF Corp.), distilled water, hydrochloric acid (HCl, 37%, Sigma-Aldrich), copper nitrate (Cu(NO₃)₂·3H₂O, 99.9%, Sigma-Aldrich), and gallium nitrate (Ga(NO₃)₃·xH₂O, 99.9%, Sigma-Aldrich). For the cinnamaldehyde hydrogenation, the chemicals were also used as purchased: trans-cinnamaldehyde (C₆H₅C₃H₃O, 98%, Merck) as reagent and isopropanol (C₃H₈O, 99.9%, Sigma-Aldrich) as solvent.

2.2. Materials synthesis

SBA-15 ordered mesoporous silica support was synthesized according to the procedure proposed by

Zhao *et al.* [43]. 4 g of Pluronic P123 surfactant was first dissolved in a 1.6 M HCl solution at 40 °C. Then, 8.5 g of TEOS was added dropwise to the surfactant solution, and the mixture was kept under magnetic stirring for 24 h. The resulting gel was subjected to hydrothermal treatment at 100 °C for 48 h. After recovering by filtration, washing, and drying, the as-made mesoporous silica was calcined in a muffle oven under stagnant air at 550 °C for 6 h (heating rate of 1.5 °C·min⁻¹) to completely remove the surfactant.

SBA-15-supported catalysts were prepared by incipient wetness impregnation using aqueous solutions of copper and gallium nitrates, followed by mild drying (25 ± 1 °C under air for 5 days), according to our earlier reported IWI-MD method [22]. The impregnates were submitted to calcination in a muffle oven under stagnant air at 500 °C for 6 h (heating rate of 1.5 °C·min⁻¹) in order to obtain the oxide forms of catalysts. The metallic forms of copper catalysts were obtained by reduction under hydrogen flow (1 L·h⁻¹) at 500 °C for 10 h (heating rate of 6 °C·min⁻¹). The nominal Cu loading was kept constant at 5 wt%, whereas the nominal Ga loadings were set at 1.0 and 2.5 wt%, resulting in two different Cu/Ga weight ratios of 5 and 2. Accordingly, the samples were labeled as CuGa₅/SBA-15 and CuGa₂/SBA-15, respectively. A Ga-free Cu/SBA-15 sample was also prepared by the same method and used as a reference material.

2.3. Materials characterisation

Inductively coupled plasma optical emission spectrometry (ICP-OES) was performed on a Perkin sequential scanning spectrometer to determine the loadings of copper and gallium in the catalysts. Before analysis, a known amount of calcined sample was introduced in a diluted HF-HCl solution and then digested under microwave.

Powder X-ray diffraction (XRD) at high-angle was performed on a Bruker AXS D5005 X-ray diffractometer, using Cu K_α radiation (λ = 1.54184 Å). Data were collected in the 2θ range 10°–80° with a step of 0.05° (step time of 8 s). Phase identification was made by comparison with the ICDD database. The average size of CuO crystallites was calculated with the Scherrer equation applied to the most intense diffraction lines at 35.5° and 38.7°.

Nitrogen physisorption at –196 °C was carried out on an Autosorb 1-MP automated gas sorption system from Quantachrome. Prior to analyses, the calcined samples were outgassed under high vacuum at 350 °C for 3 h. Being thermally stable and presenting zeolite-like intrawall micropores beside the mesopores, the calcined SBA-15—derived materials should be outgassed at temperatures above 200 °C (ideally 350–400 °C) to clean the surface from any adsorbed impurity (mainly water) [44]. The textural properties were calculated from the corresponding isotherms using conventional algorithms (BET for specific surface area, *t*-plot method for micropore surface area and NL-DFT for pore size distribution). The normalized BET surface areas of the solids were also calculated, taking into account the weight fraction of the oxide phases [45].

Transmission electronic microscopy (TEM) coupled with *energy-dispersive X-ray spectroscopy* (EDXS) was used to characterize the pore structure, the distribution of NPs throughout the mesopores of SBA-15, and their local elemental compositions, respectively. The micrographs were obtained on a JEOL 2100 instrument (operated at 200 kV with a LaB₆ source and equipped with a Gatan Ultra scan camera). EDXS was carried out with a Hypernine (Premium) detector (active area: 30 mm²) using the software SM-JED 2300T for data acquisition and treatment. Before analysis, the sample was included in a resin and crosscuts of ~100 nm were made by ultramicrotomy.

Temperature-programmed reduction (H₂-TPR) and *N₂O chemisorption* analyses were performed on a ChemBet Pulsar TPR/TPD/TPO instrument from Quantachrome. About 30 mg of calcined samples were loaded into a U-shaped microreactor. Before TPR runs, the oxidic forms of catalysts were activated at 500 °C for 1 h under a flow of simulated air (40 mL·min⁻¹). After cooling down to 50 °C, the H₂-containing flow was stabilized (40 mL·min⁻¹, 5 vol.% H₂ in Ar) and the thermo-programmed reduction was made from 50 to 850 °C, with a heating rate of 5 °C·min⁻¹. The dispersion of metallic copper (*D*_{Cu}) and active surface area (*S*_{Cu}) were determined by nitrous oxide chemisorption using the Quantachrome instrument, as reported elsewhere [46,47]. To this end, 30 mg of samples were introduced in the microreactor. The first reduction run was carried out under the same conditions as described above for

TPR, but up to 500 °C. The H₂-containing gas was then switched to Ar, the reactor was cooled down to 60 °C, and maintained isothermally for 30 min. Then, the Ar gas was switched to N₂O (40 mL·min⁻¹) for 30 min in order to oxidize the accessible Cu⁰ surface species to Cu₂O. The sample was again flushed with pure Ar for 30 min, and a second TPR run was performed to reduce surface Cu₂O to Cu⁰.

2.4. Catalytic testing

The oxidic forms of catalysts were first crushed and sieved to select a granulometric fraction smaller than 0.126 mm to ensure that the reaction rate is not limited by intragranular diffusion. The solids were then reduced under hydrogen flow in order to obtain the metallic copper catalysts. Cinnamaldehyde hydrogenation was performed in liquid phase in a high-pressure 4593 Parr reactor under the following conditions: reaction temperature of 110 °C, 1 mL of trans-cinnamaldehyde, 40 mL of isopropanol, 250 mg of catalyst, H₂ pressure of 10 bar, stirring rate of 750 rpm. It is also to be noted that preliminary experiments showed that at this high stirring rate, the reaction rate is not limited by external diffusion. Aliquots of reaction mixture were periodically taken and analyzed by GC (HP 5890 system equipped with a DB-5 capillary column and a FID detector). Identification of the reactants and products was achieved from the retention times of pure compounds, and occasionally by GC-MS (Agilent 6890N system equipped with an Agilent 5973 MSD detector and a DB-5-ms column). The total conversion of cinnamaldehyde and selectivities to the different hydrogenation products were calculated by taking into account the FID response factors for the compounds, according to a previous study [19].

3. Results and discussion

3.1. Structural and textural properties of the Cu–Ga₂O₃/SBA-15 materials

In this study, the IWI-MD method using aqueous solutions of copper and gallium nitrates was applied to introduce 5 wt% Cu, besides 1, and 2.5 wt% Ga, respectively, on ordered mesoporous SBA-15 silica support. Elemental chemical analyses by ICP-OES confirmed that the Cu and Ga loadings as well as the

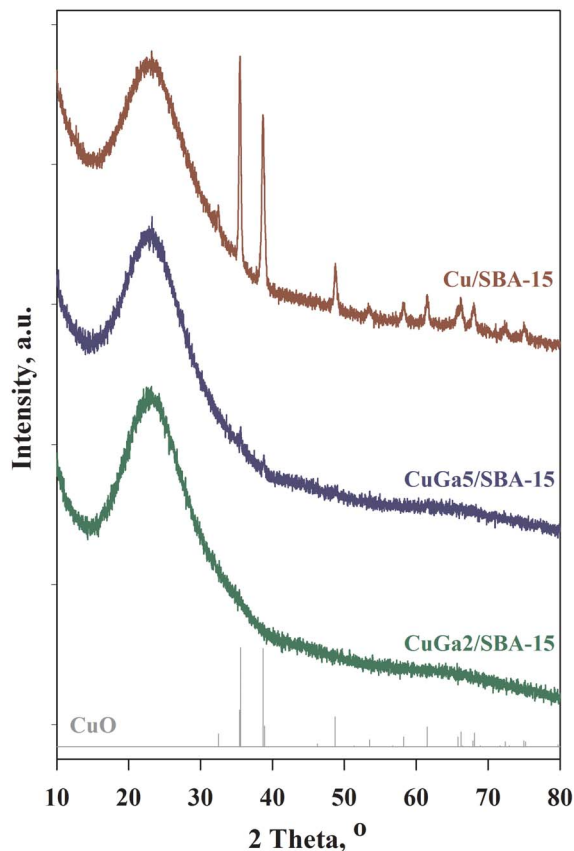


Figure 1. XRD patterns for the calcined Cu/SBA-15 and Cu–Ga₂O₃/SBA-15 materials.

Cu/Ga weight ratios are close to the nominal values (Table 1).

XRD patterns at high-angles for the calcined SBA-15-supported Cu and Cu–Ga materials are presented in Figure 1. As first observation, all the samples show broad lines at $2\theta \sim 24^\circ$, characteristic of amorphous silica. The diffractogram of the Ga-free Cu/SBA-15 sample exhibits intense and narrow diffraction lines in the range $2\theta = 30^\circ\text{--}80^\circ$, consistent with the presence of a monoclinic CuO phase (ICDD 048-1548). Calculations with the Scherrer equation disclosed that the CuO crystallites are large (mean size of 30.9 nm), and therefore, they might be found as extraporous particles, given the pore size of mesoporous SBA-15 support (8.4 nm). With the introduction of only 1 wt% Ga to Cu, the diffraction lines assigned to CuO become hardly distinguishable (CuGa₅/SBA-15), whereas for the sample containing the highest amount of Ga (CuGa₂/SBA-15), no diffraction lines

Table 1. Chemical composition and textural properties for the calcined SBA-15, Cu/SBA-15 and Cu-Ga₂O₃/SBA-15 materials

Sample	ICP-OES			N ₂ physisorption				
	Cu wt%	Ga wt%	Cu/Ga weight ratio	S _{BET} ^b (m ² ·g ⁻¹)	S _{micro} ^c (m ² ·g ⁻¹)	V _p ^d (cm ³ ·g ⁻¹)	V _{micro} ^e (cm ³ ·g ⁻¹)	D _p ^f (nm)
SBA-15	—	—	—	801	181	1.11	0.080	8.4
Cu/SBA-15	4.6	0	∞	752 (0.99)	163	1.07	0.073	8.4
CuGa ₅ /SBA-15	4.8	0.9	5.3	635 (0.85)	126	0.93	0.059	8.2
CuGa ₂ /SBA-15	4.9	2.3	2.1 (2.3 ^a)	610 (0.83)	99	0.91	0.045	8.2

^a Cu/Ga weight ratio evaluated with EDXS/TEM.

^b S_{BET} = specific surface area calculated with BET equation. The normalized BET surface area (NSA) is shown in brackets and italic as calculated using the equation: NSA = S_{catalyst} / (1 - x) · S_{SBA-15} [45], where x = weight fraction of the oxide phases calculated by elemental analysis, wt%.

^c S_{micro} = micropore surface area obtained by the *t*-method (de Boer statistical thickness = 0.38–0.65 nm).

^d V_p = total pore volume at P/P₀ = 0.97.

^e V_{micro} = micropore volume obtained by the *t*-method.

^f D_p average diameter of the main mesopores evaluated with NL-DFT for cylindrical pores (equilibrium model).

can be observed. Therefore, for the catalysts with added Ga, copper oxide is present under the form of highly dispersed NPs, with a size in the small range, below the detection limit in XRD (~3 nm) [48]. Furthermore, no diffraction lines typical to crystalline gallium oxide phases, like Ga₂O₃ or CuGa₂O₄ spinel can be seen in the diffractograms of bicomponent Cu–Ga materials, indicating their dispersed and/or amorphous state. These results should be considered as first proof that gallium oxide, even in a minimum amount, can function as an efficient structural promoter which improves the dispersion and stability of copper precursor species, as compared with the monometallic Cu catalyst.

The sample with the maximum Ga content in the series was further analyzed by TEM/EDXS. It is important to note that our previous microscopy studies on the Cu/SBA-15 materials obtained by IWI-MD showed that at a metal loading close to 5 wt%, only bulky CuO aggregates (sizes of 30–100 nm) outside the support mesopores can be formed, due to the high instability of copper precursors on the silica surface of SBA-15 [17–19,27]. Representative TEM images for the calcined CuGa₂/SBA-15 material are illustrated in Figure 2 at low (A) and high magnification (B–D). As first observation, all images exhibit typical highly-ordered mesoporous SBA-15 structures com-

posed of cylindrical mesochannels with a narrow size distribution. In excellent agreement with XRD, no extraporous oxide aggregates, nor nanoparticles within the pores of SBA-15, can be observed in the TEM images, even at a high magnification (Figures 2A and B). Nevertheless, when local elemental composition was evaluated by EDXS in the mesostructured zones of CuGa₂/SBA-15, both Cu and Ga elements were simultaneously detected, with an average Cu/Ga weight ratio of 2.3, in good agreement with the bulk Cu/Ga ratio of 2.1 (Table 1). These interesting results suggest on the one hand, the formation of highly dispersed oxide nanoparticles selectively occluding the intrawall pores of SBA-15 [24,27,49] and, on the other hand, a close proximity and a possible strong interaction between the homogeneously distributed Cu and Ga, probably due to the formation of CuO–Ga₂O₃ mixed oxides throughout the pores of the CuGa₂/SBA-15 catalyst. As reported by Yang *et al.* [49], once the NPs are encapsulated in the intrawall pores of SBA-15, they can be visualized in the high-magnification TEM images by exposing the samples to the electron beam in microscope to enhance the contrast between silica and the metal oxides. Indeed, upon exposure for at least 60 s, very small NPs of 1.5–2 nm in size can be found preferentially located within the intrawall pores and/or at

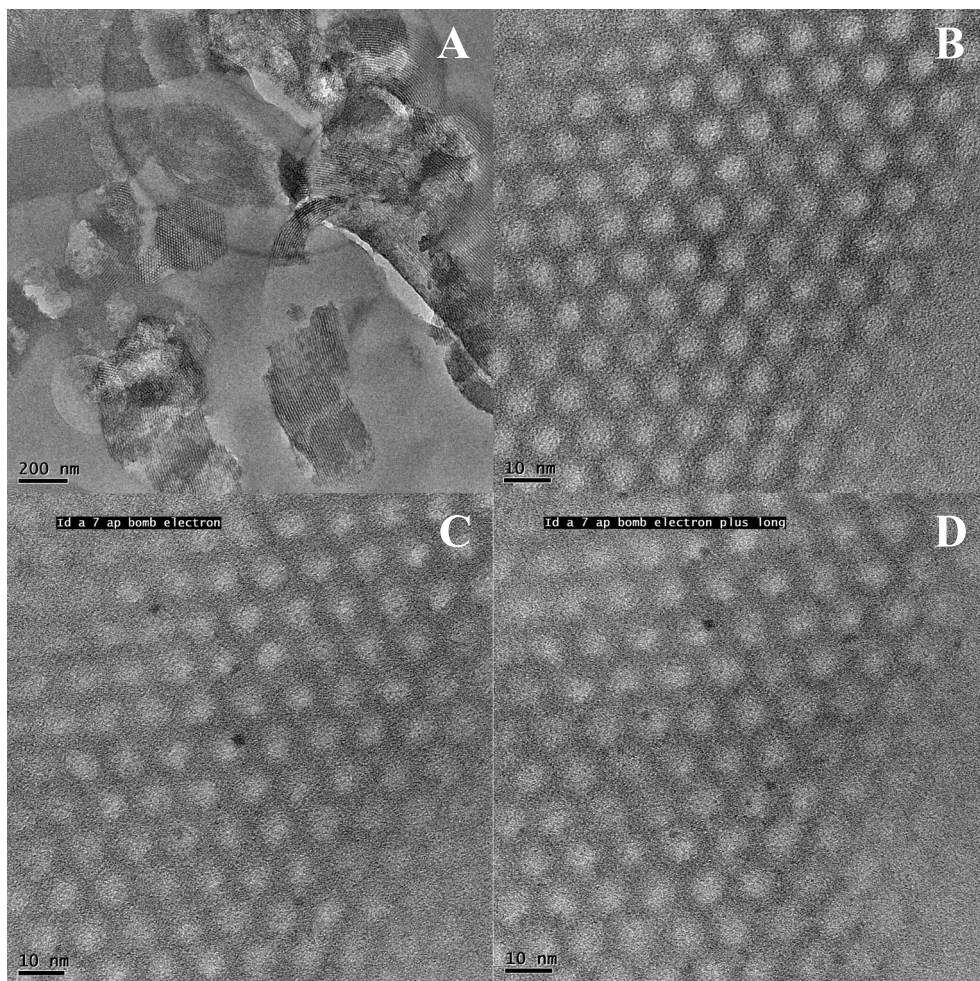


Figure 2. TEM images for the calcined $\text{CuGa}_2/\text{SBA-15}$ sample: before (A and B) and upon exposure to the electron beam in microscope: $t = 60$ s (C) and $t = 120$ s (D).

their pore mouths (Figures 2C and D), coherent with the growth of NPs by a possible partial reduction of oxidic phases under the beam.

The textural properties of the calcined SBA-15-supported Cu and Cu–Ga materials were determined by nitrogen adsorption/desorption. It is important to note that, according to the pore models described by Galarneau *et al.* [50], the SBA-15 materials synthesized in hydrothermal conditions at a temperature of 100 °C (as in the present study) actually display a dual pore system composed of primary mesopores with a pore diameter of ~8 nm and secondary pores (i.e., intrawall pores) with variable diameters in the range 1.5–4 nm (micropores and small mesopores), irregularly distributed in the framework, and inter-

connecting the adjacent primary mesopores. The isotherms and the NL-DFT pore size distributions are displayed in Figures 3A and B, together with those of the parent SBA-15. All the samples exhibit isotherms of type IV with hysteresis loops of type H1, which are characteristic for the ordered mesoporous SBA-15 materials with a narrow size distribution of the primary mesochannels [51]. The catalysts display isotherms similar in shape with the parent SBA-15, characterized by steep adsorption/desorption branches, uniform hysteresis loops, and the absence of effects due to the plugging of primary mesopores by confined particles [17,52]. For the samples containing copper and gallium, the capillary condensation steps appear slightly shifted at lower

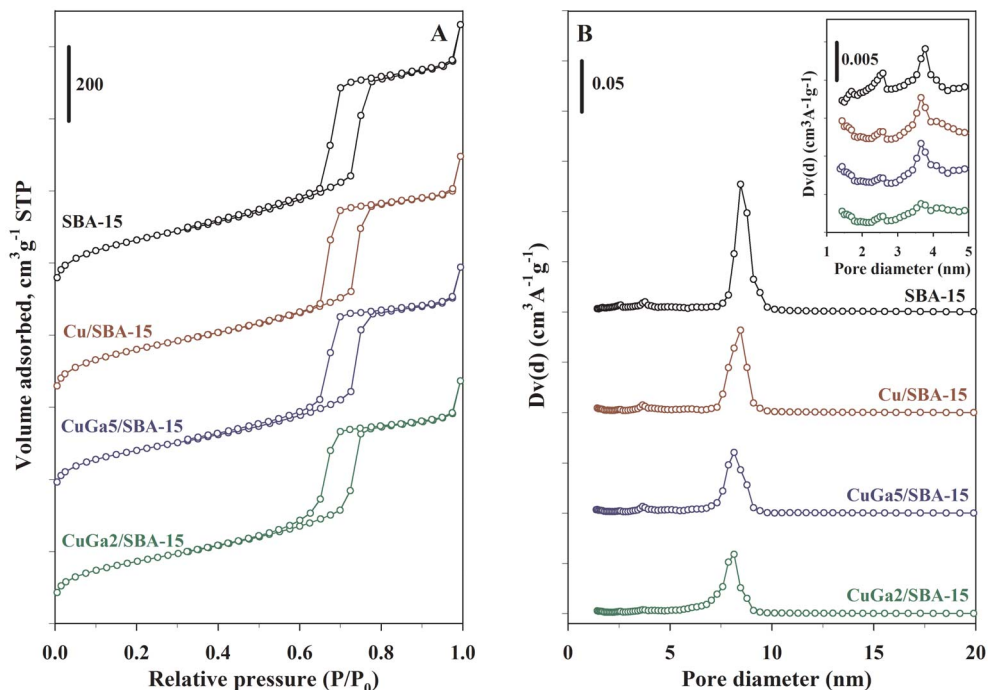


Figure 3. N₂ physisorption isotherms (A) and NL-DFT pore size distribution (B) for the calcined SBA-15, Cu/SBA-15 and Cu–Ga₂O₃/SBA-15 materials.

relative pressures, as compared with SBA-15 and Cu/SBA-15, coherent with a minor decrease in the size of primary mesopores from 8.4 to 8.2 nm (Table 1, Figure 3B). On the other hand, as illustrated in the inset of Figure 3B, the intrawall pores are indeed irregularly distributed for all the samples, encompassing pores with sizes of ~1.5 nm (micropores) and ~2.5 and ~3.7 nm, respectively (small mesopores). The volume of those intrawall pores appears to decrease from SBA-15 to CuGa₂/SBA-15, coherent with their occlusion with the highly dispersed Cu–Ga oxide NPs.

In well agreement with XRD and TEM, these results indicate the retention of the open mesoporosity of the support, given that the pores are essentially empty of CuO particles (case of Cu/SBA-15) or filled with highly dispersed CuO–Ga₂O₃ NPs located inside the intrawall pores and/or at their pore mouths (case of CuGa₅/SBA-15 and CuGa₂/SBA-15). Accordingly, as compared with SBA-15, BET surface area decreased obviously for the Cu–Ga materials, following the increase of the Ga content (Table 1), from 801 to 635, and 610 m²·g⁻¹, whereas the de-

crease is moderate for the monometallic Cu/SBA-15 sample (752 m²·g⁻¹). The micropore surface area also decreased with the increase in the Ga content, from 181 m²·g⁻¹ (SBA-15) down to 99 m²·g⁻¹ (CuGa₂/SBA-15). These trends are consistent with the decrease of the total pore volume and micropore volume from 1.11 and 0.080 cm³·g⁻¹ to 0.91 and 0.045 cm³·g⁻¹, respectively (Table 1). To further evaluate the occlusion of the SBA-15 pores by the Cu–Ga oxide NPs, the normalized BET surface areas of the catalysts (NSA) were calculated (Table 1), values around unity giving an indication of less pore occlusion [45]. The Cu/SBA-15 material displays a BET NSA of 0.99, showing essentially no pore occlusion because the pores are empty of CuO phases. Compared with Cu/SBA-15, the samples CuGa₅/SBA-15 and CuGa₂/SBA-15 show BET NSAs smaller than unity (0.85 and 0.83, respectively), coherent with the presence of the highly dispersed Cu–Ga NPs occluded within/at the mouth of the SBA-15 intrawall pores.

Overall, XRD, TEM/EDXS and N₂ physisorption results clearly demonstrate that the introduction of

gallium to copper onto the high-surface area micro-mesoporous silica SBA-15 support by simple impregnation prevented the migration and particle growth of copper upon calcination, resulting in small and stable Cu–Ga oxide NPs, located inside the pores. It is postulated that CuO–Ga₂O₃ oxides have suffered the nucleation and growth inside/at the mouth of these small micro-mesoporous domains, generating stable intrawall pore-encapsulated metal oxide crystallites. In addition, the Cu–Ga materials display open mesopores with a narrow size distribution as well as an excellent textural uniformity, which should favor efficient molecule mass-transfer, in view of their use in catalysis. Earlier studies on other bicomponent Cu–Ga materials indicated that maximizing Cu–Ga₂O₃ interactions is key to prevent the aggregation of copper particles, allowing to increase the metal dispersion, and thus the active surface area of catalysts [33,34]. Conversely, further studies concluded that Ga₂O₃ increases the number of active sites by enhancing Cu dispersion [35,36], yet other authors reported no positive effect of Ga₂O₃ addition on the dispersion of Cu NPs supported on silica [37]. It was also suggested that the Ga₂O₃ particles supported on mesoporous silica supports can act as strong anchoring sites for the Cu species, leading to a better dispersion, as compared with the monometallic Cu materials [38]. It was stressed that the dispersion of Ga₂O₃ should be equally high to create a high interfacial area between the oxide promoter and the metallic Cu NPs [40].

3.2. Reducible properties of Cu–Ga₂O₃/SBA-15 materials

H₂-TPR experiments were performed for all the calcined nanocatalysts in order to study the reducibility of copper precursor species and confirm their properties in terms of dispersion and interaction with gallium (Figure 4). The TPR profile for the monometallic Cu/SBA-15 shows one broad hydrogen consumption peak with a maximum at ~290 °C, typical for the reduction of large CuO aggregates located outside the SBA-15 mesoporosity [19]. For the samples containing copper and gallium, the reduction profiles become more complex, characterized by two peaks at temperatures lower than 500 °C and

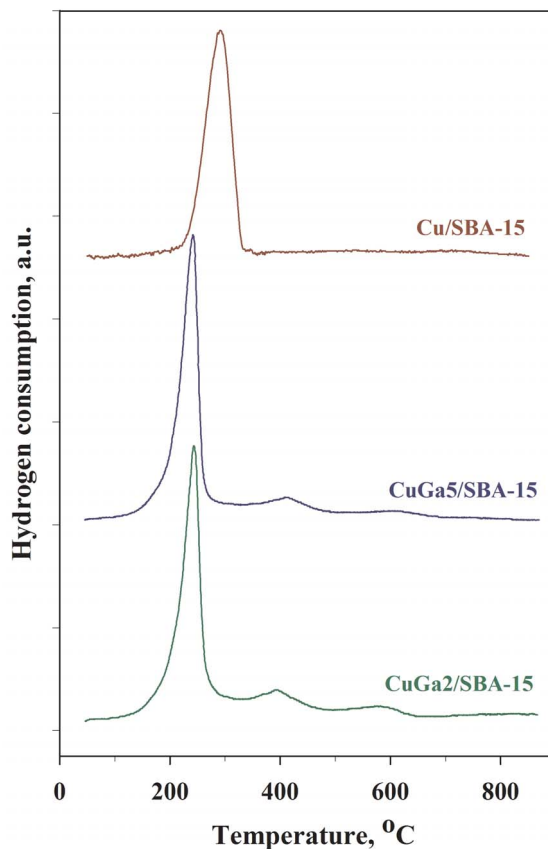


Figure 4. H₂-TPR profiles for the calcined Cu/SBA-15 and Cu–Ga₂O₃/SBA-15 materials.

one peak at higher temperatures. It should be mentioned that the experimental hydrogen consumptions at 500 °C are in good agreement with the theoretical ones, considering the actual Cu loadings (16.9 and 17.2 cm³·g⁻¹ for CuGa₅/SBA-15 and CuGa₂/SBA-15, respectively), and therefore, the two reduction peaks recorded up to 500 °C essentially reflect the complete reduction to zero-valent copper of those Cu²⁺ species displaying different degrees of interaction with the gallium oxide. While the first narrow peaks at ~240 °C for both Cu–Ga samples are unambiguously assigned to the reduction of the highly dispersed CuO NPs [24,26,27], the second peaks (~415 and ~395 °C for CuGa₅/SBA-15 and CuGa₂/SBA-15, respectively) might be assigned to the reduction of Cu²⁺ in a strong interaction with Ga₂O₃, most likely in CuGa₂O₄ spinel nanophases formed upon calcination [33,34,53]. Indeed, Faungnawakij *et al.* [53] re-

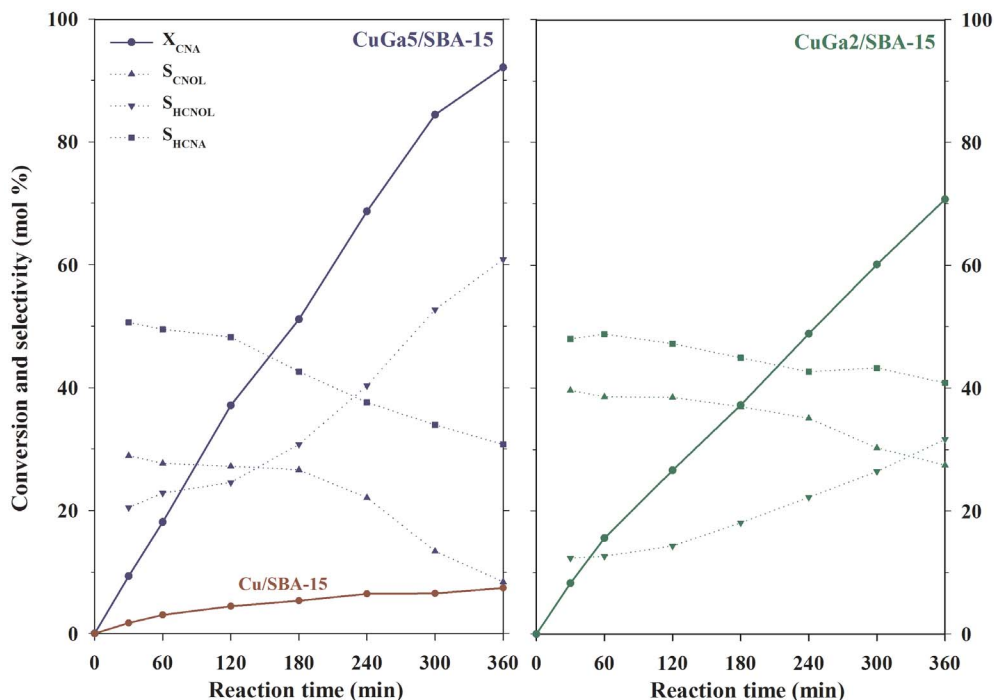


Figure 5. Cinnamaldehyde conversion and product selectivity as a function of the reaction time for the Cu-Ga₂O₃/SBA-15 catalysts. Reaction conditions: $T_{\text{reduction}} = 500\text{ }^{\circ}\text{C}$; $T_{\text{reaction}} = 110\text{ }^{\circ}\text{C}$; 250 mg of catalyst; 1 mL of CNA, 40 mL of isopropanol; $P_{\text{H}_2} = 10\text{ bar}$; stirring rate = 750 rpm.

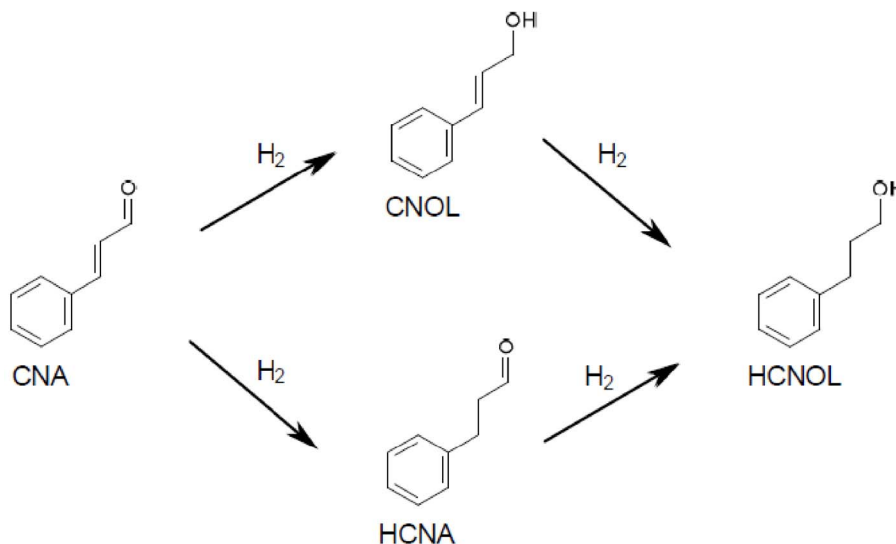
ported that the CuGa₂O₄ nanospinel can be reduced over a wide temperature range of 300–500 °C, with the formation of Cu⁰ and Ga₂O₃. At higher temperatures, CuGa₅/SBA-15 and CuGa₂/SBA-15 display reduction peaks at ~620 and ~585 °C, respectively, assigned to the reduction of Ga³⁺ to Ga⁺ in well dispersed Ga₂O₃ NPs, according to previous studies focused on Ga₂O₃ supported on porous oxides (ZSM-5, SBA-15, γ -Al₂O₃, and SiO₂) [32]. Overall, the TPR results for the bicomponent Cu-Ga materials show that the reduction at 500 °C leads to highly dispersed Cu⁰ sites along with remaining Ga³⁺ sites. Based on the hydrogen consumptions at higher temperatures, it is anticipated that the number of the Ga³⁺ sites increases with the loading of Ga. Considering these aspects, for the catalytic experiments, the reduction temperature of the catalysts was set at 500 °C.

3.3. Catalytic properties of Cu-Ga₂O₃/SBA-15 materials

The catalytic performances of the reduced forms of the SBA-15-supported Cu and Cu-Ga catalysts were

evaluated in the liquid phase hydrogenation of cinnamaldehyde (CNA). This reaction involves several hydrogenation pathways, with the formation of hydrocinnamaldehyde (HCNA) and cinnamyl alcohol (CNOL) as primary hydrogenated products, and of hydrocinnamyl alcohol (HCNOL) as the completely hydrogenated product (Scheme 1). It is to be noted that the preferred pathway on most catalysts, including the silica-supported Cu catalysts, is the C=C bond hydrogenation due to favorable thermodynamics and lower activation barriers [26–28].

The conversion of cinnamaldehyde (X_{CNA}) as a function of reaction time is shown in Figure 5. The Ga-free Cu/SBA-15 sample showed no significant conversion, even after 360 min of reaction, but the introduction of Ga to Cu increased X_{CNA} for both catalysts (Table 2). Thus, X_{CNA} outstandingly increased from 8% for the unpromoted Cu catalyst to 92% for CuGa₅/SBA-15. Interestingly, the conversion further decreased to 71% for the catalyst with more Ga in composition (CuGa₂/SBA-15). Compared with the catalyst without Ga, the presence of a minimum



Scheme 1. Reaction pathways in the hydrogenation of cinnamaldehyde (CNA). CNOL: cinnamyl alcohol, HCNA: hydrocinnamaldehyde, HCNOL: hydrocinnamyl alcohol.

amount of Ga (Cu/Ga = 5) hence improved the catalytic activity, under the same reaction conditions, whereas an excess of Ga (Cu/Ga = 2) then decreased the activity.

Because the metallic copper atoms are the only species involved in the activation of H₂, one may anticipate that the catalytic activity in the cinnamaldehyde hydrogenation depends on the dispersion and, consequently, on the accessible surface area of copper. Therefore, N₂O chemisorption was applied for all the catalysts to elucidate the effect of Cu/Ga weight ratio on the dispersion of copper upon reduction at 500 °C (Table 3). As expected on the basis of above XRD, TEM and H₂-TPR results, the unpromoted Cu/SBA-15 displayed the lowest dispersion in the series (4.6%, $1.4 \text{ m}_{\text{Cu}}^2 \cdot \text{g}_{\text{cat}}^{-1}$). Remarkably, the dispersion increased nine-fold for the sample CuGa₅/SBA-15 (39.3%, $12.8 \text{ m}_{\text{Cu}}^2 \cdot \text{g}_{\text{cat}}^{-1}$) and then, it decreased for the sample CuGa₂/SBA-15 with the maximum amount of Ga (32.1%, $10.6 \text{ m}_{\text{Cu}}^2 \cdot \text{g}_{\text{cat}}^{-1}$), consistent therefore with the measured catalytic activity. The evolutions in both Cu dispersion and activity in the hydrogenation of cinnamaldehyde over the Cu–Ga catalysts with different Cu/Ga weight ratios are evidences of the possible changes in the Cu–Ga₂O₃ phases upon reduction, mainly in the surface concentration of exposed Cu. Thus, it is postulated that the lower number of exposed Cu sites for the

CuGa₂/SBA-15 catalyst compared with CuGa₅/SBA-15 is due to a partial blocking of surface Cu atoms by Ga₂O₃ nanophases. Similar phenomena have been put in evidence in the case of other metal–metal oxide catalytic promoted systems, such as the Pt–Fe and Pt–Ga catalysts for the hydrogenation of citral [29,30], and the Cu–Mn catalysts for the hydrogenation of ethyl acetate [54].

Based on the N₂O chemisorption results, the specific activity of the catalysts was further evaluated as the initial turnover frequency (TOF, expressed in mol of CNA converted per mol of surface copper per unit time). The results are shown in Table 2. The initial TOF increased from $1.9 \times 10^{-3} \text{ s}^{-1}$ for Cu/SBA-15 to $4.9 \times 10^{-3} \text{ s}^{-1}$ for CuGa₅/SBA-15, while remaining at a similar level of $5.1 \times 10^{-3} \text{ s}^{-1}$ for CuGa₂/SBA-15. These results indicate that the intrinsic catalytic activity of the surface copper sites in the hydrogenation of cinnamaldehyde over the Cu–Ga catalysts does not essentially depend on the Cu/Ga weight ratio. It is also important to note that both Cu–Ga catalysts are among the most active supported copper nanocatalysts reported in literature. For example, under similar reaction conditions, a TOF of $3 \times 10^{-3} \text{ s}^{-1}$ was obtained for Cu/SiO₂ (12 wt% Cu), whilst $2 \times 10^{-3} \text{ s}^{-1}$ was reported for Cu/MCM-14 (21 wt% Cu) [55]. These TOF values are in the same range as the value shown by the poorly dispersed Cu/SBA-15 catalyst. By com-

Table 2. Catalytic performances for the Cu/SBA-15 and Cu–Ga₂O₃/SBA-15 catalysts

Catalyst	Catalytic activity ^a		Catalytic selectivity ^c		
	X _{CNA} ^a (mol%)	TOF × 10 ³ ^b (s ⁻¹)	S _{CNOL} (mol%)	S _{HCNA} (mol%)	S _{HCNOL} (mol%)
Cu/SBA-15	8	1.9	—	—	—
CuGa ₅ /SBA-15	92	4.9 (5.1 ^d)	27 (28 ^d)	48 (49 ^d)	25 (23 ^d)
CuGa ₂ /SBA-15	71	5.1	38	45	17

^aX_{CNA} = conversion of CNA measured after 360 min of reaction.

^b TOF = initial turnover frequency based on the initial reaction rate, in mol of CNA converted per mol of surface copper per unit time, calculated using N₂O chemisorption.

^cSelectivity evaluated at ~40 mol% isoconversion of CNA.

^dData from Dragoi *et al.* [27] for the highly-dispersed Cu/SBA-15 catalyst (5 wt% Cu, D_{Cu} = 69.5%).

Table 3. N₂O chemisorption data for the reduced Cu/SBA-15 and Cu–Ga₂O₃/SBA-15 materials

Sample	D _{Cu} ^b (%)	S _{Cu} ^c (m ² _{Cu} ·g _{cat} ⁻¹)	S _{Cu} ^c (m ² _{Cu} ·g _{Cu} ⁻¹)
Cu/SBA-15 ^a	4.6	1.4	31.1
CuGa ₅ /SBA-15 ^a	39.3	12.8	265.9
CuGa ₂ /SBA-15 ^a	32.1	10.6	217.2

^aT_{reduction} = 500 °C.

^bD_{Cu} = dispersion of metallic Cu.

^cS_{Cu} = accessible surface area of metallic Cu.

parison, the initial TOF values found in this study for the Cu–Ga catalysts are close to the value of $5.1 \times 10^{-3} \text{ s}^{-1}$ reported previously for Cu NPs supported on SBA-15 partially occluded with the P123 surfactant (5 wt% Cu, D_{Cu} = 69.5%, Cu particle size = 1.4 nm) [27], and of $6 \times 10^{-3} \text{ s}^{-1}$ for Cu NPs supported on Al-SBA-15 (5 wt% Cu, D_{Cu} = 25.6%, Cu particle size = 3.9 nm) [19].

The selectivity of the Cu–Ga catalysts to the different hydrogenation products (S_{CNOL}, S_{HCNA}, and S_{HCNOL}) as a function of the reaction time and conversion of cinnamaldehyde is illustrated in Figure 5. At the initial stages of reaction (X_{CNA} = 10%), the preferred pathway for both catalysts was first the C=C bond hydrogenation with the formation of HCNA (S_{HCNA} = 50%) and then, the C=O bond hydrogenation with the formation of CNOL (S_{CNOL} = 30% for CuGa₅/SBA-15 and 40% and CuGa₂/SBA-15). With the increase of X_{CNA}, the selectivity to those pri-

mary hydrogenation products decreased owing to their subsequent hydrogenation, consistent with the increase of S_{HCNOL}. However, at all conversion levels, the selectivity to CNOL is higher for CuGa₂/SBA-15 than CuGa₅/SBA-15, whereas the selectivity to HCNA is comparable, signifying that a higher amount of Ga is favorable for the hydrogenation of C=O bonds. The selectivity values are presented in Table 2 at X_{CNA} = 40%. Thus, CuGa₅/SBA-15 showed selectivity typical to divided monometallic copper catalysts (S_{CNOL} = 27%, S_{HCNA} = 48%, and S_{HCNOL} = 25%). For example, similar levels of selectivity at X_{CNA} = 40% have been reported for an unpromoted Cu/SBA-15 catalyst comprising highly dispersed Cu NPs of 1.4 nm in size (S_{CNOL} = 28%, S_{HCNA} = 49%, and S_{HCNOL} = 23%) [27]. These results suggest that at Cu/Ga = 5, Ga₂O₃ does not bring enough electron deficient sites to modify the competition between the adsorption of C=C and C=O groups of cinnamaldehyde molecules on the copper catalyst surface such that the C=O hydrogenation be favored. Nevertheless, at Cu/Ga = 2, S_{CNOL} is improved by 11% compared with CuGa₅/SBA-15, mostly at the expense of the decrease of S_{HCNOL} (S_{CNOL} = 38%, S_{HCNA} = 45%, and S_{HCNOL} = 17%). Overall, it is believed that with the increase of the Ga₂O₃ content, the number of surface Ga^{δ+} species functioning as Lewis acid sites becomes higher [38,39]. Such Ga ionic species located in the neighbouring of the active Cu⁰ sites could hence polarize the carbonyl groups of the cinnamaldehyde molecules, facilitating their hydrogenation and improving the selectivity to the unsaturated alcohol [30]. More detailed investigations con-

cerning the effect of Lewis acidity (i.e., nature, density and strength of acid sites) on the chemoselectivity of supported Cu nanocatalysts in the hydrogenation of cinnamaldehyde are currently underway for a series of SBA-15-supported Cu-MO_x nanoparticles (M = Al, Ga, and Fe).

4. Conclusions

Ga₂O₃-promoted Cu/SBA-15 catalysts with a constant Cu loading (5 wt%) and two different Ga loadings (Cu/Ga weight ratio of 2 and 5) were prepared by incipient wetness impregnation followed by mild drying and their catalytic performances were evaluated for the hydrogenation of cinnamaldehyde relative to the unpromoted Cu/SBA-15 catalyst. The introduction of gallium promoter to copper afforded small Cu-Ga₂O₃ nanoparticles and much higher metallic Cu dispersions, and active surface areas (up to 39.3%, and 12.8 m²_{Cu} g⁻¹_{cat}), finally leading to a superior catalytic activity (TOF of ~5 × 10⁻³ s⁻¹), when compared with the poorly dispersed Cu/SBA-15 catalyst (TOF of 1.9 × 10⁻³ s⁻¹). Besides, it was found that the selectivity to the unsaturated cinnamyl alcohol increases with the amount of gallium up to a level of 38% at 40% conversion, an effect that was ascribed to the presence of electron deficient Ga^{δ+} sites with affinity for the C=O groups of the cinnamaldehyde molecules.

Conflicts of interest

Authors have no conflict of interest to declare.

Acknowledgments

This work was supported by a grant of the Romanian National Authority for Scientific Research, CNCS-UEFISCDI (Project PN-II-RU-TE-2012-3-0403). The Chevreul Institute is thanked for its help in the development of this work through the ARCHI-CM project supported by the “Ministère de l’Enseignement Supérieur de la Recherche et de l’Innovation”, the region “Hauts-de-France”, the ERDF program of the European Union and the “Métropole Européenne de Lille”. S. Arrii-Clacens and S. Pronier (IC2MP UMR 7285, CNRS, Université de Poitiers) are acknowledged for XRD and TEM analyses, respectively.

References

- [1] L. Liu, A. Corma, *Chem. Rev.*, 2018, **118**, 4981-5079.
- [2] L. Zhang, M. Zhou, A. Wang, T. Zhang, *Chem. Rev.*, 2020, **120**, 683-733.
- [3] P. Munnik, P. E. de Jongh, K. P. de Jong, *Chem. Rev.*, 2015, **115**, 6687-6718.
- [4] J. M. Campelo, D. Luna, R. Luque, J. M. Marinas, A. A. Romero, *ChemSusChem*, 2009, **2**, 18-45.
- [5] B. R. Cuenya, *Thin Solid Films*, 2010, **518**, 3127-3150.
- [6] L. De Rogatis, M. Cargnello, V. Gombac, B. Lorenzut, T. Montini, P. Fornasiero, *ChemSusChem*, 2010, **3**, 24-42.
- [7] N. Wang, Q. Sun, J. Yu, *Adv. Mater.*, 2019, **31**, article no. 1803966.
- [8] M. B. Gawande, A. Goswami, F. X. Felpin, T. Asefa, X. Huang, R. Silva, X. Zou, R. Zboril, R. S. Varma, *Chem. Rev.*, 2016, **116**, 3722-3811.
- [9] R.-P. Ye, L. Lin, Q. Li, Z. Zhou, T. Wang, C. K. Russell, H. Adidharma, Z. Xu, Y.-G. Yao, M. Fan, *Catal. Sci. Technol.*, 2018, **8**, 3428-3449.
- [10] R. Watari, Y. Kayaki, *Asian J. Org. Chem.*, 2018, **7**, 2005-2014.
- [11] P. Gallezot, D. Richard, *Catal. Rev. Sci. Eng.*, 1998, **40**, 81-126.
- [12] P. Mäki-Arvela, J. Hájek, T. Salmi, D. Y. Murzin, *Appl. Catal. A Gen.*, 2005, **292**, 1-49.
- [13] X. Lan, T. Wang, *ACS Catal.*, 2020, **10**, 2764-2790.
- [14] X. Wang, X. Liang, P. Geng, Q. Li, *ACS Catal.*, 2020, **10**, 2395-2412.
- [15] P. Munnik, M. Wolters, A. Gabrielsson, S. D. Pollington, G. Headdock, J. H. Bitter, P. E. de Jongh, K. P. de Jong, *J. Phys. Chem. C*, 2011, **115**, 14698-14706.
- [16] T. W. Hansen, A. T. Delariva, S. R. Challa, A. K. Datye, *Acc. Chem. Res.*, 2013, **46**, 1720-1730.
- [17] A. Ungureanu, B. Dragoi, A. Chiriac, C. Ciotonea, S. Royer, D. Duprez, A. S. Mamede, E. Dumitriu, *ACS Appl. Mater. Interfaces*, 2013, **5**, 3010-3025.
- [18] B. Dragoi, A. Ungureanu, A. Chiriac, V. Hulea, S. Royer, E. Dumitriu, *Catal. Sci. Technol.*, 2013, **3**, 2319-2329.
- [19] A. Ungureanu, A. Chiriac, C. Ciotonea, I. Mazilu, C. Catrinescu, S. Petit, E. Marceau, S. Royer, E. Dumitriu, *Appl. Catal. A Gen.*, 2020, **598**, article no. 117615.
- [20] C. Ciotonea, A. Chiriac, B. Dragoi, J. Dhainaut, M. Marinova, S. Pronier, S. Arii-Clacens, J.-P. Dacquin, E. Dumitriu, A. Ungureanu, S. Royer, *Appl. Catal. A Gen.*, 2021, **623**, article no. 118303.
- [21] T. Toupance, M. Kermarec, C. Louis, *J. Phys. Chem. B*, 2000, **104**, 965-972.
- [22] A. Ungureanu, B. Dragoi, A. Chiriac, S. Royer, D. Duprez, E. Dumitriu, *J. Mater. Chem.*, 2011, **21**, 12529-12541.
- [23] C. H. Liu, N. C. Lai, J. F. Lee, C. S. Chen, C. M. Yang, *J. Catal.*, 2014, **316**, 231-239.
- [24] A. Chiriac, B. Dragoi, A. Ungureanu, C. Ciotonea, I. Mazilu, S. Royer, A. S. Mamede, E. Rombi, I. Ferino, E. Dumitriu, *J. Catal.*, 2016, **339**, 270-283.
- [25] C. Rudolf, I. Mazilu, A. Chiriac, B. Dragoi, F. Abi-Ghaida, A. Ungureanu, A. Mehdi, E. Dumitriu, *Environ. Eng. Manag. J.*, 2015, **14**, 399-408.
- [26] C. Rudolf, F. Abi-Ghaida, B. Dragoi, A. Ungureanu, A. Mehdi, E. Dumitriu, *Catal. Sci. Technol.*, 2015, **5**, 3735-3745.
- [27] B. Dragoi, I. Mazilu, A. Chiriac, C. Ciotonea, A. Ungureanu,

- E. Marceau, E. Dumitriu, S. Royer, *Catal. Sci. Technol.*, 2017, **7**, 5376-5385.
- [28] A. J. Marchi, D. A. Gordo, A. F. Trasarti, C. R. Apesteguía, *Appl. Catal. A Gen.*, 2003, **249**, 53-67.
- [29] J. P. Stassi, P. D. Zgolicz, S. R. de Miguel, O. A. Scelza, *J. Catal.*, 2013, **306**, 11-29.
- [30] J. P. Stassi, P. D. Zgolicz, V. I. Rodríguez, S. R. de Miguel, O. A. Scelza, *Appl. Catal. A Gen.*, 2015, **497**, 58-71.
- [31] C. Louis, L. Delannoy, *Adv. Catal.*, 2019, **64**, 1-88.
- [32] C.-T. Shao, W.-Z. Lang, X. Yan, Y.-J. Guo, *RSC Adv.*, 2017, **7**, 4710-4723.
- [33] K. M. K. Yu, W. Tong, A. West, K. Cheung, T. Li, G. Smith, Y. Guo, S. C. E. Tsang, *Nat. Commun.*, 2012, **3**, article no. 1230.
- [34] P. B. Sanguineti, M. A. Baltanás, A. L. Bonivardi, *Appl. Catal. A Gen.*, 2015, **504**, 476-481.
- [35] S. Natesakhawat, J. W. Lekse, J. P. Baltrus, P. R. Ohodnicki, B. H. Howard, X. Deng, C. Matranga, *ACS Catal.*, 2012, **2**, 1667-1676.
- [36] R. Ladera, F. J. Pérez-Alonso, J. M. González-Carballo, M. Ojeda, S. Rojas, J. L. G. Fierro, *Appl. Catal. B Env.*, 2013, **142-143**, 241-248.
- [37] J. C. Medina, M. Figueroa, R. Manrique, J. R. Pereira, P. D. Srinivasan, J. J. Bravo-Suárez, V. G. B. Medrano, R. Jiménez, A. Karelavic, *Catal. Sci. Technol.*, 2017, **7**, 3375-3387.
- [38] A. M. Hengne, K. D. Bhatte, S. Ould-Chikh, Y. Saih, J. M. Basset, K.-W. Huang, *ChemCatChem*, 2018, **21**, 1360-1369.
- [39] E. Lam, G. Noh, K. W. Chan, K. Larmier, D. Lebedev, K. Searles, P. Wolf, O. V. Safonova, C. Copéret, *Chem. Sci.*, 2020, **11**, 7593-7598.
- [40] C. Paris, A. Karelavic, R. Manrique, S. Le Bras, F. Devred, V. Vykoukal, A. Styskalik, P. Eloy, D. P. Debecker, *ChemSusChem*, 2020, **13**, 6409-6417.
- [41] J. Du, Y. Zhang, K. Wang, F. Ding, S. Jia, G. Liu, L. Tan, *RSC Adv.*, 2021, **11**, 14426-14433.
- [42] D. Verma, R. Insyani, H. S. Cahyadi, J.-Y. Park, S. M. Kim, J. M. Chao, J. W. Bae, J. Kim, *Green Chem.*, 2018, **20**, 3253-3270.
- [43] D. Zhao, J. Feng, Q. Huo, N. Melosh, G. H. Fredrickson, B. F. Chmelka, G. D. Stucky, *Science*, 1998, **279**, 548-552.
- [44] A. Figini-Albisetti, L. F. Velasco, J. B. Parra, C. O. Ania, *Appl. Surf. Sci.*, 2010, **256**, 5182-5186.
- [45] L. Vradman, M. V. Landau, D. Kantorovich, Y. Koltypin, A. Gedanken, *Microporous Mesoporous Mater.*, 2005, **79**, 307-318.
- [46] A. Gervasini, S. Bennici, *Appl. Catal. A Gen.*, 2005, **281**, 199-205.
- [47] G. V. Sagar, P. V. R. Rao, C. S. Srikanth, K. V. R. Chary, *J. Phys. Chem. B*, 2006, **110**, 13881-13888.
- [48] S. Mourdikoudis, R. M. Pallares, N. T. K. Thanh, *Nanoscale*, 2018, **10**, 12871-12934.
- [49] C. M. Yang, H. A. Lin, B. Zibrowius, B. Spliethoff, F. Schüth, S. C. Liou, M. W. Chu, C. H. Chen, *Chem. Mater.*, 2007, **19**, 3205-3211.
- [50] A. Galarneau, H. Cambon, F. Di Renzo, R. Ryoo, M. Choi, F. Fajula, *New J. Chem.*, 2003, **27**, 73-79.
- [51] M. Kruk, M. Jaroniec, *Chem. Mater.*, 2001, **13**, 3169-3183.
- [52] J. R. A. Sietsma, J. D. Meeldijk, M. Versluijs-Helder, A. Broersma, A. J. van Dillen, P. E. de Jongh, K. P. de Jong, *Chem. Mater.*, 2008, **20**, 2921-2931.
- [53] K. Faungnawakij, N. Shimoda, T. Fukunaga, R. Kikuchi, K. Eguchi, *Appl. Catal. A Gen.*, 2008, **341**, 139-145.
- [54] R. Beerthuis, N. L. Visser, J. E. S. van der Hoeven, P. Ngene, J. M. S. Deeley, G. J. Sunley, K. P. de Jong, P. E. de Jongh, *J. Catal.*, 2021, **394**, 307-315.
- [55] V. Gutierrez, M. Alvarez, M. A. Volpe, *Appl. Catal., A Gen.*, 2012, **413-414**, 358-365.